Available online at www.sciencedirect.com
SCIENCE DIRECT®

Journal of the European Ceramic Society 23 (2003) 1361–1368

www.elsevier.com/locate/jeurceramsoc

Room and elevated temperature strength of perovskite membrane tubes

N. Nagendra*, S. Bandopadhyay

School of Mineral Engineering, University of Alaska, Fairbanks, Fairbanks, AK 99775, USA

Received 3 January 2002; received in revised form 3 June 2002; accepted 23 September 2002

Abstract

Lanthanum-based perovskite oxides are promising materials as membranes for oxygen separation and for direct oxidation of gaseous hydrocarbons. The physical and mechanical properties of these oxide membranes are however dependent on the temperature and environment. In the present study, two differing sets of oxide membrane tubes were evaluated for their fracture strength in a C-ring geometry in three different conditions: room temperature in air and at 1000 °C in air and nitrogen. The strength of the oxide tubes in ambient conditions was observed to be dependent on the processing route (initial composition, surface and volume flaws). With a change in temperature and environment from ambient to reducing condition, the strength degraded to nearly half its initial value. The strength degradation was accompanied by decomposition of the membranes and changes in fracture mode and morphology. The strength degradation as measured by mean strength and Weibull parameters and changes in fracture characterized by Scanning Electron Microscopy (SEM) and X-ray diffractometry (XRD) are reported.

Keywords: Fracture; (La,Sr)(Fe,Cr)O_3; Mechanical properties; Membranes; Perovskites; Scanning electron microscopy

1. Introduction

Perovskite-type oxides that combine a high electronic and ionic conductivity are very promising materials for potential use as dense ceramic membranes for oxygen separation, solid oxide fuel cells etc.[1–4] Lanthanum-based perovskites are indeed being used in membrane reactors that can produce synthetic gas ($CO + H_2$) by direct conversion of hydrocarbons such as methane. Important issues in the development of perovskite-type oxygen conducting membranes for converting reactors are the structural, chemical and mechanical stability of the materials at high temperatures and in reducing environments. Many of the physical properties of perovskite oxides, including the oxygen transport properties are related to the oxygen stoichiometry, which depends on temperature and oxygen partial pressure.[5–8] Among the various oxides evaluated, the transition metal perovskite-type oxides (ABO_3) with La, Sr at the A site and the B site primarily occupied by transition elements Fe, Cr and Co are seen to be of commercial interest. These $A_xA'_{1-x}B_yB'_{1-y}O_3$ oxides (A = La, A′ = Ba, Sr, Ca; B = Cr, Co, B′ = Fe, Mn) show both a high oxygen ionic conductivity due to high oxygen vacancy concentration and a high electronic conductivity due to a mixed-valence state.[9] The oxides are reportedly stable in reducing atmosphere with oxygen permeability of 1–2 magnitudes greater than conventional stabilized Zirconia.[1]

For gas separation of interest, the structural design and reactor efficiency deem that the oxide membranes are used as tubes (rather than as bars, rods or plates) in the reactors with air flowing along the inner side and the gas stream on the outer surface. The reactor environments viz. high temperature, pressure and reducing conditions are to be expected to significantly influence the mechanical properties of the oxide membranes. Evaluation of reliable mechanical properties of the oxide membranes in its operating conditions is thus of much importance for successful design of a gas separation unit. However, mechanical properties on perovskite oxides (Gallates, Chromites, etc. from fuel cells literature) obtained from laboratory testing of regular specimens such as bend bars[10–17] are not expected to give a good estimate for design purposes since the tubular

* Corresponding author.
E-mail address: ffnn@uaf.edu (N. Nagendra).

0955-2219/03/$ - see front matter © 2003 Elsevier Science Ltd. All rights reserved.
PII: S0955-2219(02)00367-9

geometry can be subject to a much more complex levels of thermal and mechanical stresses. With this broad objective in mind, C-ring tests [18,19] were chosen for strength evaluation of oxide membrane tubes. For a C-ring test, the specimen preparation is simple and since the maximum tensile stress is generated along the outer diameter, results are sensitive to surface flaws or changes in surface flaw distribution induced by environmental factors. In this paper, initial results on the strength and fracture characteristics of two different sets of commercially produced Cr_2O_3 doped $LaSrFeO_3$ perovskite membrane tubes are presented. The tests are done at room temperature in air, and at 1000 °C in air and in a slightly reducing atmosphere (log $pO_2 = -4$) and fracture was examined by scanning electron microscopy.

2. Experimental procedure

Cr_2O_3 doped $LaSrFeO_3$ perovskite membrane tubes of the general composition $La_{0.2}Sr_{0.8}Fe_{0.8}Cr_{0.2}O_{3-\delta}$ (LSFCO), processed by a proprietary process involving cold-isostatic pressing of the base powder and sintering at 1500 °C in N_2 were provided for testing. Two sets of tubes (LSFCO-1 and LSFCO-2 respectively), differing in their initial powder preparation and the final particle size were tested. The tubes were characterized for hardness and fracture toughness by indentation technique.[20] Indentation loads of 10 g–1 kg were applied by a mechanical indentor with a 10-s residence time and the associated radial cracks were measured. A total of five indentations were averaged at each load to determine the hardness and fracture toughness.

Rings of dimension as shown in Table 1 were cut from them and to maintain dimensional uniformity in samples, the ratio of the width to the outer diameter of the rings were kept at a constant value of 0.9. The surfaces were polished and the edges beveled to prevent edge failures. The rings were notched by a 0.5-mm low speed saw to form a C-ring specimen.[18,19] The C-rings were placed in an autoclave (to ensure uniform temperature and humidity) between two alumina platens in a hydraulic testing frame (MTS 858 MiniBionix II). Stabilized zirconia cloth (0.5 mm) as pressure pads were used to reduce frictional stresses and to prevent slippage of the rings during testing (Fig. 1). To ensure that the tests yielded reproducible values, initial tests were done on commercially available and surface finished alumina (99.8%) tubes. For testing in reducing conditions, the autoclave chamber was flushed with Ultra High Purity N_2 until a steady state was established and a positive chamber pressure of 0.17 MPa was maintained. The chamber temperature was then raised at 10 °C/min to the final temperature of 1000 °C and the rings soaked for a period of 15 min at the reducing conditions (log $pO_2 = -4$ atm) prior to application of load. All the tests were done by monotonic loading in diametral compression to fracture at a constant crosshead speed of 0.5 mm/min.

The maximum fracture strength of the C-Ring specimens were calculated from the equation:

$$\sigma_{\theta\max} = \frac{PR}{btr_o}\left[\frac{r_o - r_a}{r_a - R}\right] \quad (1)$$

where r_o is the outer radius of the C-Ring; b, the width; t, thickness; P, the measured fracture load; $r_a = (r_o + r_i)/2$ and $R = \{(r_o - r_i)/\ln(r_o/r_i)\}$.

Three samples were tested at each condition and for Weibull analysis a total of 12 samples were tested. The failure probability (P_f) was estimated from the expression

$$P_f = (n - 0.5)/N_t \quad (2)$$

where N_t is the total number of samples tested and n is the rank of a particular specimen. The resulting data were fitted to the two-parameter Weibull equation[21] to determine the Weibull parameter (m) and characteristic stress (σ_o). The fractured surfaces were examined under Scanning Electron Microscope (SEM), to characterize the dominating flaws and fracture mechanisms. The outer surfaces exposed to the environment were analyzed in a Siemens D5000 θ/θ diffractometer using Cu radiation at 40 kv/30 ma to determine any phases

Table 1
Sample dimensions and mechanical properties of LSFCO membrane tubes

Sample	Test condition	Outer radius (r_o), mm	Inner radius (r_i), mm	Average thickness (t), mm	Hardness, GPa	Fracture toughness, $MPa\sqrt{m}$	No. of samples (n)	Average strength, MPa	Weibull parameter, m
Alumina	Ambient	4.8	3.18	1.6	–	–	12	229	16
LSFCO-1	Ambient	5.42	4.42	1	5.2±0.5	0.5–0.8	11	167	5.2
	Air, 1000 °C						3	108	–
	N_2, 1000 °C						3	139	–
LSFCO-2	Ambient	5.75	4.65	1.1	4.4±0.5	1–1.5	12	307	4
	Air, 1000 °C						3	115	–
	N_2, 1000 °C						12	178	4.8

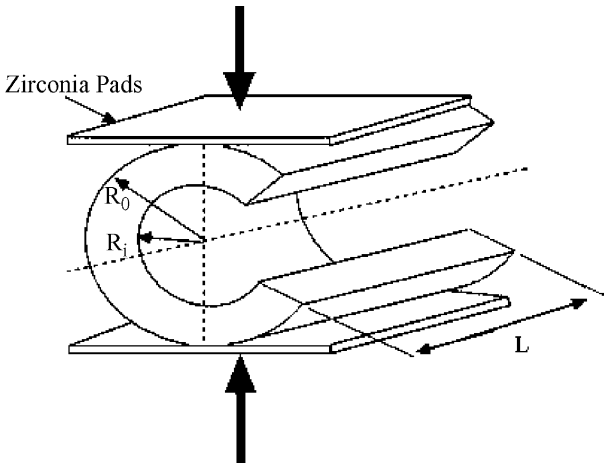

Fig. 1. Schematic of the C-ring test for strength evaluation of ceramic tubes.

formed after the tests. The samples were tested in a parallel beam arrangement to minimize the displacement errors caused by the curved surfaces.

3. Results

3.1. Mechanical properties and fracture

3.1.1. Room temperature

The room temperature hardness and indentation fracture toughness are as shown in Table 1. The hardness and indentation toughness of LSFCO-1 was in the range of 5.2±0.5 GPa and 0.5–0.8 MPaÖm respectively. In comparison, LSFCO-2 showed a slightly reduced hardness of 4.4±0.5 GPa but increased toughness of 1–1.5 *MPa*Öm respectively. In both cases, hardness was independent of indentation load and radial crack were observed at load of 100 g.

The measured strength of the $La_{0.2}Sr_{0.8}Fe_{0.8}Cr_{0.2}O_{3-\delta}$ tubes is as shown in Table 1. The recorded maximum and the average strength of sample set LSFCO-2 (429 MPa and 307 MPa respectively) were twice of that recorded in sample set LSFCO-1 (210 MPa and 167 MPa respectively). Macroscopic observation indicated a distinctive difference in fracture morphology between sets LSFCO-1 and LSFCO-2 respectively (Fig. 2). The entire specimens in set LSFCO-1 fractured at midplane and the fracture surfaces were smooth while on the other hand, specimens of set LSFCO-2 shattered during testing and very often the fracture planes were at an angle (5–10°) from the midplane. The fracture morphology was predominantly jagged with interspersing planes of smooth fracture. Subsequent microscopic analysis (Fig. 3) indicated that the fracture in both the sets of tubes was controlled primarily by the surface and volume flaws. The volume flaws were approximately of the order of 10–25 μm and occurred randomly in the microstructure. Microscopic studies also indicated that although the fracture in both the sets were by cleavage they were of distinctively different morphology. In set LSFCO-1 (Fig. 4a), the surfaces were smooth with apparent lack of features while in set LSFCO-2 (Fig. 4b) microscopic cleavage planes and pore elongation at triple point grain boundaries were observed.

3.1.2. High temperature and environment

The strength of the oxide membrane tube decreases with increase in temperature. The strength degradation was markedly more severe in air (Log $pO_2 = -0.7$ atm) in comparison with N_2 (Log $pO_2 = -4$ atm) environment. In addition, LSFCO-1 indicated a higher resistance to strength degradation in comparison with LSFCO-2. Strength of the LSFCO-1 tubes decreased from 167 MPa to 108 MPa and 139 MPa in air and N_2 respectively, while in LSFCO-2, strength decreased rapidly to nearly half its value at the ambient condition (Table 1). Significantly, all the specimens in LSFCO-1 had fractured smoothly at the midplane while the LSFCO-2 specimens had shattered and fracture was observed to have deviated significantly from the mid-plane.

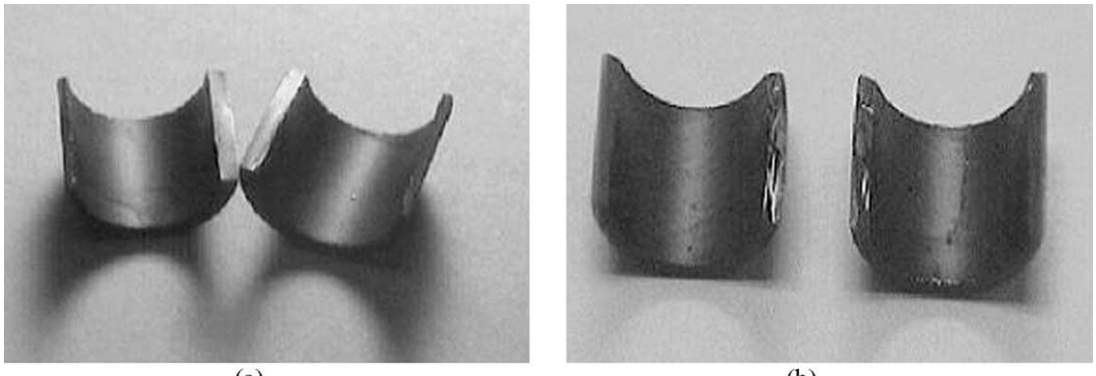

Fig. 2. Macrographs of fracture observed in the two sets of perovskite tubes: (a) featureless cleavage in LSFCO-1 and (b) jagged surfaces in LSFCO-2.

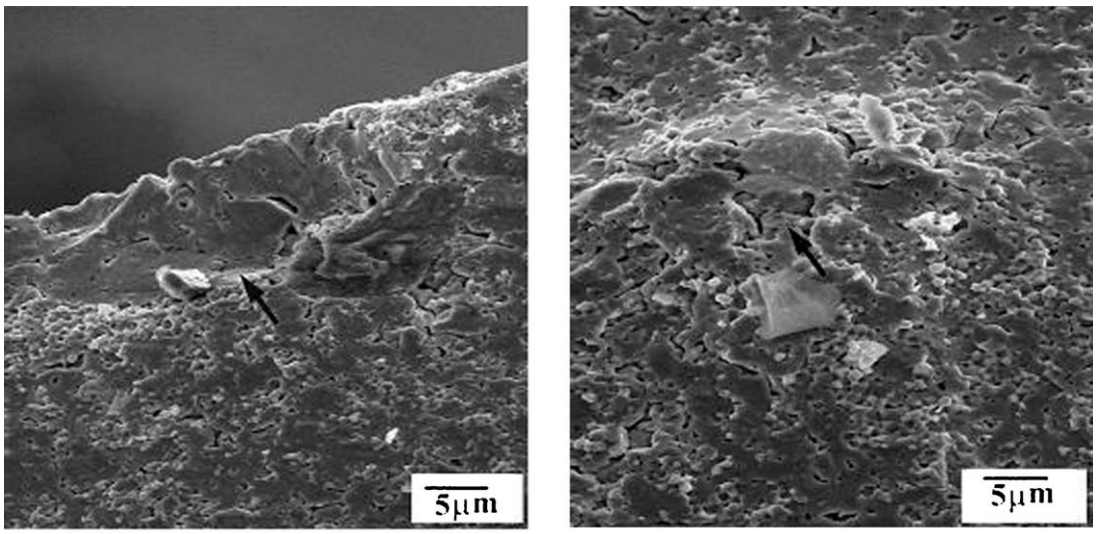

Fig. 3. SEM examination of the fracture surfaces indicating failure initiated by: (a) surface flaws and (b) volume flaws.

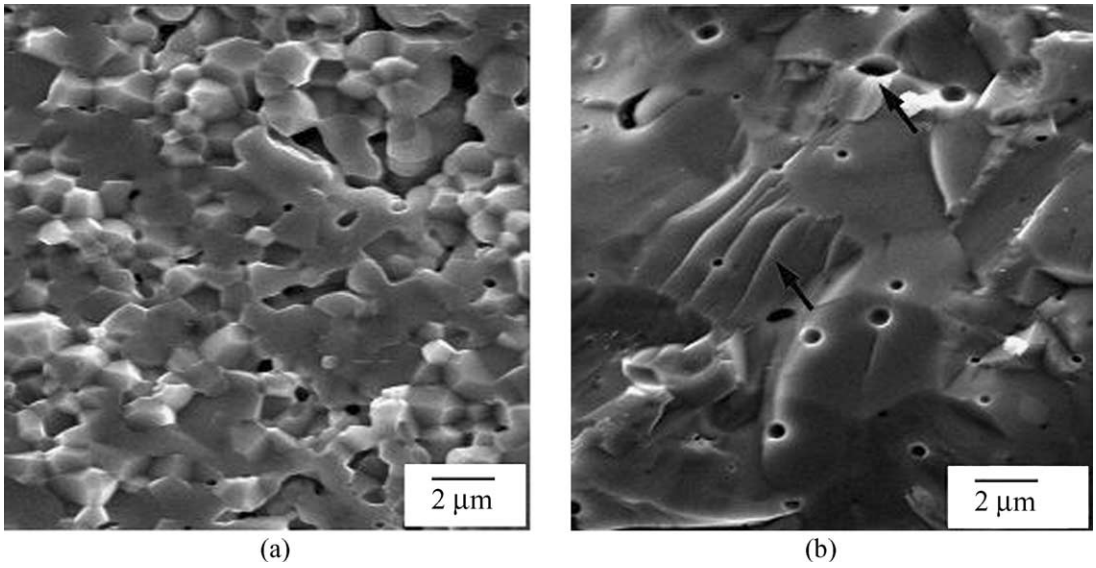

Fig. 4. Distinctive change in cleavage morphology observed in the two set of sample. In LSFCO-1 (a) the fracture is purely cleavage and in LSFCO-2 (b) particulate pull out and micro-cleavage is also observed.

Microscopic analysis indicates that volume flaws dominated the fracture origins in both the set of tubes although appreciable differences were seen in the fracture morphology. In both air and N_2, LSFCO-1 fractured in a mix of intergranular and transgranular mode (Fig. 5a), while LSFCO-2 fractured in a transgranular mode with instances of grain-boundary cavitations and pores formation at grain-boundary triple points. Additionally, in air, the fractured grains indicated the beginning of decomposition with the thickening of grain boundaries (Fig. 5b) and in N_2 decomposition manifested as an extensive relief between the grains and the grain boundaries (Fig. 5c).

3.2. X-ray analysis

At room temperature, X-ray analysis of the membranes indicated that the dominant phase in both the tubes was the primitive cubic perovskite phase. As shown in Fig. 6a and b, testing at room temperature did not alter the structure although at higher temperature traces of decomposition products were observed. In LSFCO-1 (Fig. 6a), samples tested in air at 1000 °C showed traces of (La,Sr)CrO_3 and no decomposition in N_2. On the other hand, LSFCO-2 samples (Fig. 6b) decomposed to form (La,Sr)CrO_3 and (La,Sr)$Fe_{12}O_{12}$ in air and (La,Sr)CrO_3 in N_2 respectively.

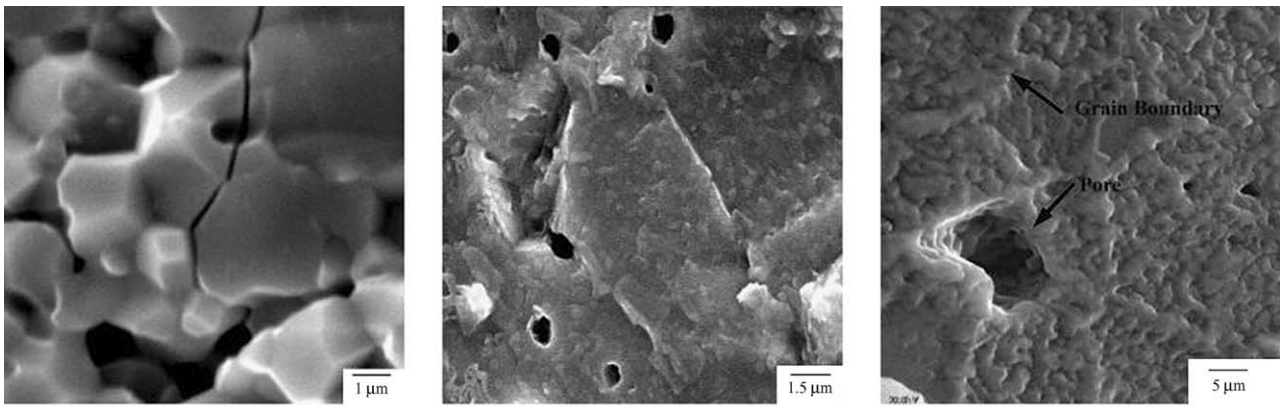

Fig. 5. Fracture observed in LSFCO at 1000 °C. (a) LSFCO-1 in air; (b) LSFCO-2 in air and (c) LSFCO-2 in 0.17 MPa N_2.

4. Discussions

The C-ring tests for ceramic tubes, which demonstrate a lower strength, are more indicative of realistic properties of the tubes as they have a larger effective volume and surface area under stress and thus statistically increase the probability of finding a flaw of critical size. The strength of the tubes plotted as a Weibull graph in Fig. 7a and b, indicate that the 'as-received' LSFCO tubes expectedly show a much lower Weibull parameter ($m = 4$–5), in comparison with surface finished alumina ($m = 16$). The lower value of 'm' in both the sample sets signifies the influence of specimen geometry and flaw distribution on the overall strength distribution. The observed variation in the Weibull parameters and strength values can be attributed to the following factors: (1) processing related flaw distribution viz. surface and volume flaws. The Weibull plots indicated a multimodal flaw distribution in both the set of tubes. However, in both the sets, the lower strengths measured corresponded to fracture originating from surface flaws. Change in the flaw distribution in individual sample set can occur due to various factors such as: additives added (distribution of volume pores arising from binder burn out), die used (surface flaws distribution) related to the processing of the tube; (2) variation observed in the wall thickness and ovality of the tubes provided. C-rings from LSFCO-1 were generally less uniform in thickness while in rings from LSFCO-2, variation in outer diameter was observed; (3) orientation of the fracture plane with respect to the loading axis or to the axis of the tube. Variation in dimension of the C-ring can significantly alter the stress distribution in the ring. Specifically in LSFCO-2, although fracture was not at the midplane, the measured angles of fracture were not too high (10–15° as compared to ~30° needed for a significant change in stress distribution) to necessitate a detailed stress distribution. The equivalency from a computed stress profile for a C-ring test indicate that the fiber strains are nearly equivalent over a region described by $\theta = 30°$ and maximum stresses are not limited to the exact midplane of the specimen [22] and (4) inherent strength of the material.

The first three factors affecting the strength distributions are invariably related to the processing route employed for processing the tubes. However, the fourth factor is a function of the composition, phases and microstructure. This is well reflected in the apparent difference between the two sets of tubes with respect to their fracture behavior and morphology. LSFCO-1 is relatively fine grained, fractured smoothly, and fracture was purely cleavage with total absence of any feature indicative of a very low energy brittle fracture. On the other hand, LSFCO-2 is coarser grained and fractured by shattering into more pieces, an indication of high-energy fracture. The fracture exhibited additional features such as micro-cleavage of grains indicating activation of toughening related mechanisms. This is complemented by the higher toughness measured in comparison with LSFCO-1 tubes.

At elevated temperatures corresponding to slightly reducing conditions (Log $_pO_2 = -0.7$ and -4 atm), the strength of the perovskite membrane tube reduces sharply in comparison with room temperature strength. Fracture and X-ray analysis of the samples indicate that the strength degradation is aided by the decomposition of the grains. In air, the strength rapidly degrades accompanied by decomposition to (La,Sr)CrO_3 and (La,Sr)$Fe_{12}O_{12}$ (in LSFCO-2). In N_2, strength degradation is less severe and is accompanied by decomposition only in the case of LSFCO-2. Line scans analysis across the fractured grains indicated that the bulk of the grain exhibited the same elemental composition as at the room temperature. However, grain boundaries were rich in strontium and the grains markedly strontium deficient. This corresponded well with previous observations concluding a build up of strontium at the grain boundaries and the strontium deficient grains acting as acceptors.[23] Fracture can be explained in greater detail by taking recourse to earlier studies involving *Z*-con-

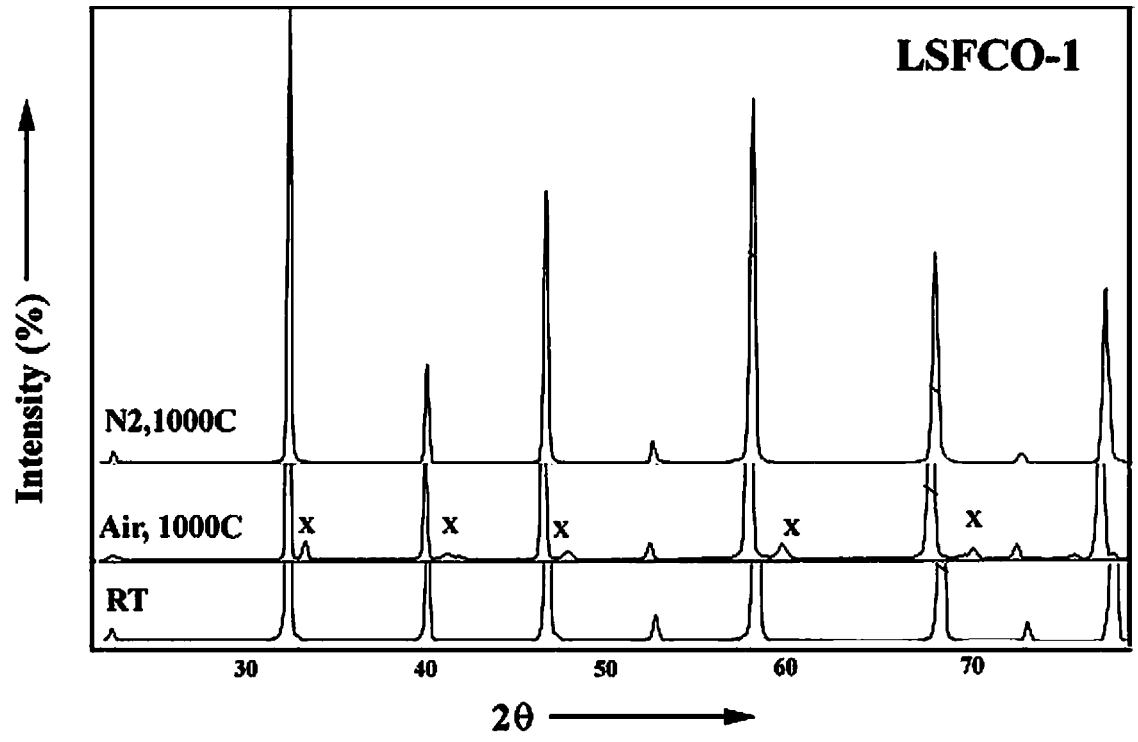

(a)

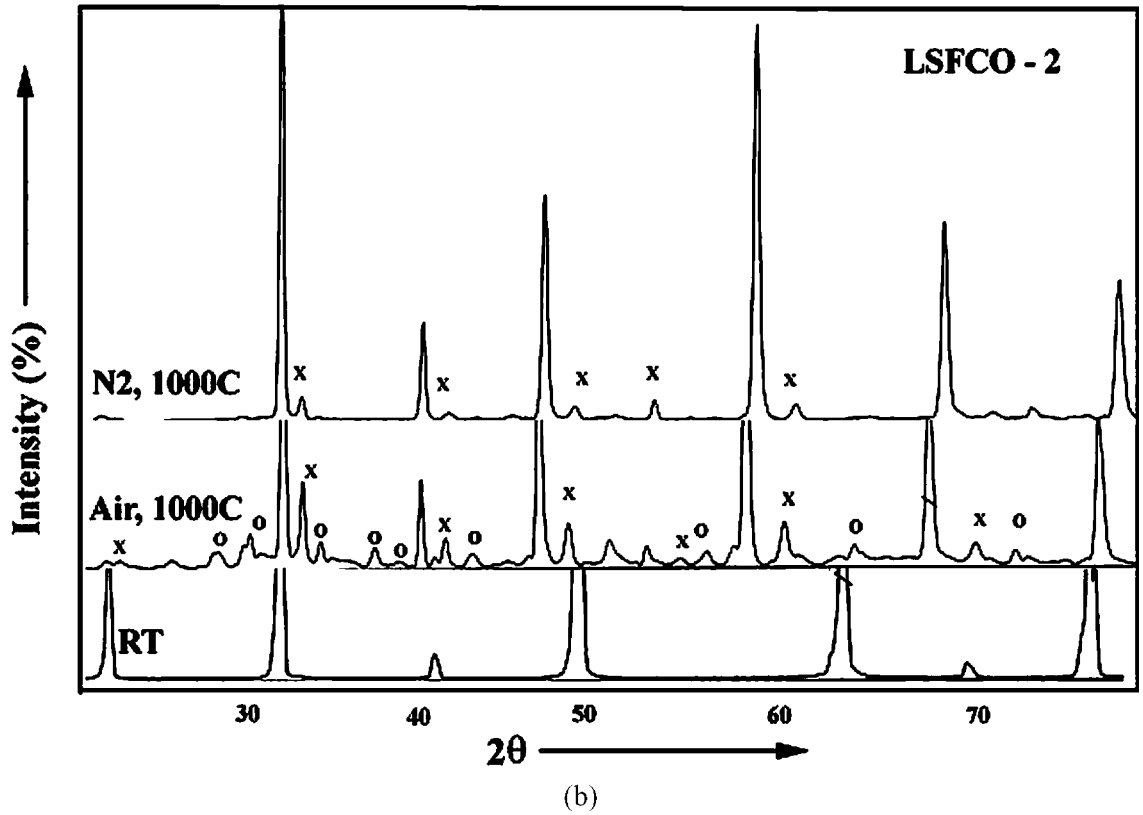

(b)

Fig. 6. X-ray analysis of C-rings surfaces after fracture: (a) LSFCO-1 and (b) LSFCO-2. The parent perovskite phase is relatively unchanged while decomposition products: **x**- $(La,Sr)CrO_3$ and **o**- $(La,Sr)Fe_{12}O_{12}$ are formed.

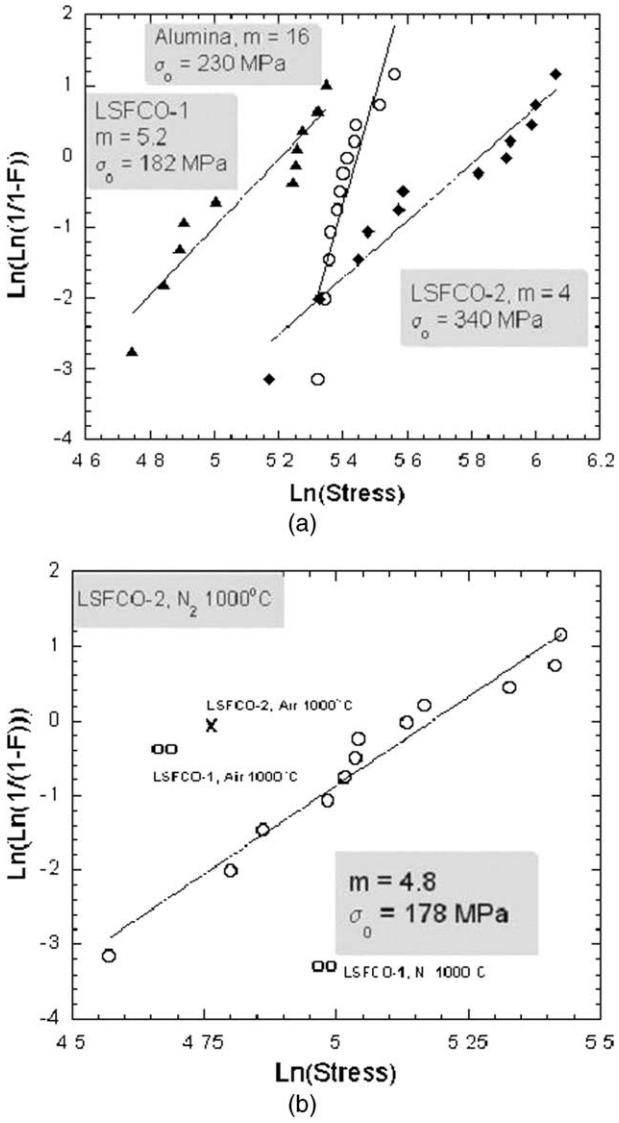

Fig. 7. Weibull plots for C-ring test at (a) ambient temperature and (b) reducing conditions (1000 °C in N_2 at 0.17 MPa).

trast transmission electron microscopy and electron energy loss spectra (EELS) on the membranes at room and elevated temperature.[24] The studies indicated that upon exposure to reducing conditions, oxygen vacancies in the perovskite underwent an ordering transition resulting in the formation of a Brownmillerite phase. The structural ordering results in a lattice expansion in one dimension (~2.6%) and introduces additional stresses in the membrane. In the present case, although the brownmillerite phase could not be distinguished by XRD patterns, the observed morphology in the grains and at the grain boundaries is suggested to relate to the segregation and decomposition induced effects and to structural transitions in the parent perovskite.[25] The decomposition can be assumed to begin with the precipitation of $(La,Sr)CrO_3$ at the grain boundary. The formation of extensive relief at the grain boundaries (Fig. 5c) is subsequently aided by the enrichment of Sr at the grain boundaries and structural transitions in the perovskite.

In the case of LSFCO-2, decrease in strength at the reducing conditions is also accompanied by a slight increase in the Weibull parameter. Although this increase from 4 at room temperature to 4.8 at elevated temperatures is not significant (the values may possibly converge with a large number of tests), there is a possibility that reducing conditions may have blunted the strength controlling surface flaws dominating at room temperature. The Weibull plot in this case appears flatter (Fig. 7b) and the strength distribution controlled by volume flaws. The volume flaws distribution can also be expected to be augmented by the additional grain boundary cavitations and pores formed at the grain boundaries.

5. Conclusions

The strength distributions and fracture in two perovskite oxide membrane tubes of the composition $La_{0.2}Sr_{0.8}Fe_{0.8}Cr_{0.2}O_{3-\delta}$ are reported. The membrane tubes evaluated by C-ring strength tests show low Weibull parameter (m) of 4–5, which can be attributed to the effects of specimen geometry, surface and volume flaw distribution. Fractures in both the tubes were by brittle transgranular cleavage. The fine-grained LSFCO-1 had a much lower strength and toughness in comparison with coarse-grained LSFCO-2. However, the additional increment in strength and toughness in LSFCO-2 was offset by poor dimensional control resulting in lowered Weibull parameter.

In comparison with LSFCO-2 tubes, LSFCO-1 tubes exhibited more resistance to strength degradation in both air and N_2. The strength degradation in both the tubes was accompanied by changes in fracture behavior and decomposition that was markedly severe in air. In LSFCO-1, fracture was a mix of intergranular and transgranular mode, while in LSFCO-2, fracture was essentially transgranular with extensive relief observed between individual grains. X-ray analysis indicated that the membranes retained their basic perovskite structure with additional formation of $(La,Sr)CrO_3$ and (La,Sr)-$Fe_{12}O_{12}$ as decomposition products. Line scan analyses across fractured grains indicate that decomposition would have started at the strontium rich grain boundaries.

Acknowledgements

This research was sponsored by the National Energy Technology Laboratory, US Department of Energy under grant number DE-FC26-99FT40054. We thank T.J. Mazanec and W.T. Stephens for providing the samples.

References

1. Teraoka, Y., Zhang, H. M., Okamato, K. and Yamazoe, N., *Mater. Res. Bull.*, 1988, **23**, 51.
2. Balachandran, U., Dusek, J. T., Sweeney, S. M., Poeppel, R. B., Mieville, R. L., Maiya, P. S., Kleefish, M., Pei, S., Kobylinski, T. P., Udovich, C. A. and Bose, A. C., *Ceram. Bull.*, 1995, **74**(1), 71–75.
3. Tsai, C. Y., Dixon, A. G., Ma, Y. H., Moser, W. R. and Pascussi, M. R., *J. Am. Ceram. Soc.*, 1998, **81**, 1437–1444.
4. Stevenson, J. W., Armstrong, T. R., Carneim, R. D., Pederson, L. R. and Weber, W. J., *J. Electrochem. Soc.*, 1996, **143**, 2722–2729.
5. Huang, K., Tichy, R. S. and Goodenough, J. B., *J. Am. Ceram. Soc.*, 1998, **81**, 2565–2675.
6. Mazanec, T. J., *Solid State Ionics*, 1994, **70/71,** 11.
7. Anderson, M. T., Haughey, J. T. and Poeppelmeier, K. R., *J. Am. Ceram. Soc.*, 1993, **3**, 151.
8. Rao, C. N. R., Gopalkrishanan, J. and Vidyasagar, K., *Ind. J. Chem.*, 1984, **23A**, 265.
9. Mizusaki, J., Yoshihiro, M., Yamauchi, S. and Feiki, K., *J. Solid State Chem.*, 1985, **58**, 257–266.
10. Sammes, N. M., Ratnaraj, R. and Fee, M. G., *J. Mater. Sci.*, 1994, **29**, 4319.
11. Sammes, N. M. and Ratnaraj, R., *J. Mater. Sci.*, 1995, **30**, 4523.
12. Sammes, N. M., Keppeler, F. M., Näfe, H. and Aldinger, F., *J. Am. Ceram. Soc.*, 1998, **81**, 3104–3108.
13. Paulik, S. W., Baskaran, S. and Armstrong, T. R., *J. Mater. Sci.*, 1998, **33**, 2397.
14. Stevenson, J. W., Armstrong, T. R., Pederson, L. R., Li, J., Lewinsohn, C. A. and Baskaran, S., *Solid State Ionics*, 1998, **113–115**, 571.
15. Baskaran, S., Lewinsohn, C. A., Chou, Y. S., Qian, M., Stevenson, J. W. and Armstrong, T. R., *J. Mater. Sci.*, 1999, **34**, 3913.
16. Paulik, S. W., Baskaran, S. and Armstrong, T. R., *J. Mater. Sci. Lett.*, 1999, **18**, 819.
17. D'Souza, C. M. and Sammes, N. M., *J. Am. Ceram. Soc.*, 2000, **83**, 47–52.
18. Ferber, M. K., Tennery, V. J., Walters, S. and Ogle, J. C., *J. Mater. Sci.*, 1986, **8,** 2628.
19. ASTM C 1323-96, *American Society for Testing and Materials*, 1996, **547**.
20. Anstis, G. R., Chantikul, P., Lawn, B. R. and Marshall, D. B., *J. Am. Ceram. Soc.*, 1981, **64**, 533.
21. Weibull, W., *J. Appl. Mech.*, 1951, **18**, 293.
22. Landini, D. J., Flinna, J. E. and Kelsey, P. V. Jr. In *Advances in Ceramics 14*, ed. B. D. Foster and J. B. Patton. The Am. Ceram. Soc. Columbus, Ohio, 1996.
23. Palanduz, A.C. private communications.
24. Klie, R. F. and Browning, N. D., *J. Electron. Microsc.*, 2002, **51**, S59–S66.
25. Nagendra, N., Klie, R.F., Browning, N.D. and Bandopadhyay, S., *Mater. Sci. Eng A*, 2002, **341**, 236.